Application of geoacoustic inference to assess the diurnal effects of photosynthetic activity in a seagrass meadow

Megan S. Ballard, Kevin M. Lee, Jason D. Sagers, Gabriel R. Venegas, and Andrew R. McNeese
Applied Research Laboratories, The University of Texas at Austin
Preston S. Wilson
Walker Department of Mechanical Engineering, The University of Texas at Austin
Abdullah F. Rahman
School of Earth, Environmental, and Marine Science, The University of Texas Rio Grande Valley

Acoustical Effects of Bubbles

Sound propagation is sensitive to the presence of bubbles which cause dispersion, absorption, and scattering of sound

- Chloroplasts in seagrass tissues use the sun's energy to convert carbon dioxide and water into sugar and oxygen for growth through the process of photosynthesis
- Gas bodies within the seagrass tissue, known as lacunae, exchange oxygen and carbon dioxide throughout the plant
- Under high irradiance, the partial pressure of oxygen contained in the lacunae can exceed that of the surrounding water, and oxygen diffuses through the plant tissue to form bubbles on the surfaces of the leaves

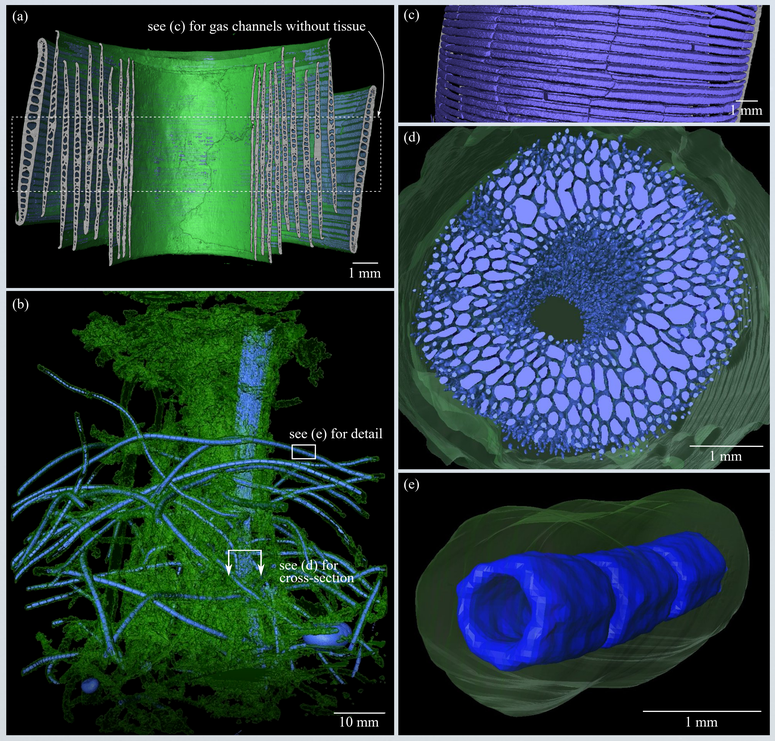

(a) CT imagery of a seagrass blade, which was curled around itself with apical end of the leaf positioned on the inside of the coil. The seagrass tissue is shown in translucent green, the lacunae are shown in blue, and the cross-section of the blade are shown in gray. (b) CT imagery of the upper 10 cm of a 7.6 cm diameter sediment core containing the vertically orientated shoot and horizontally orientated roots. The seagrass tissue is shown in translucent green, the lacunae and free gas bubbles are shown in blue. (c) Gas channels in the outer coil of the seagrass blades, tissue not shown. (d) Cross-section showing the gas volumes contained in the vertically-orientated rhizome. (e) Detailed view of the segmented tubular gas cavities in the roots.

Effective Medium Models for Bubbly Liquids

This work utilizes an effective medium model that applies a suitably chosen average to the microscopic conservation laws and introduces averaged field variables. The resulting averaged governing equations replace the complex distribution of scatterers within a host medium with a continuous effective medium (Commander and Prosperetti, 1989).
For frequencies sufficiently well below the individual bubble resonance frequency, the effective sound speed can be approximated by the Mallock-Wood equation (Mallock, 1910; Wood, 1930), which is frequency independent.

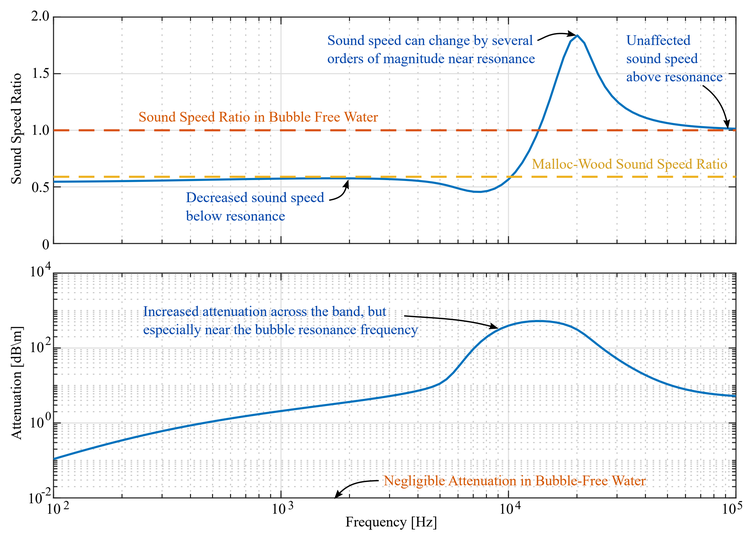

(a) Sound speed ratio (sound speed of bubbly liquid compared to that of bubble-free water) calculated using the Commander and Prosperetti (blue) and Malloc-Wood (gold) effective medium models. The sound speed ratio in bubble-free water (orange) is shown for reference. (b) Attenuation calculated using the Commander and Prosperetti model (blue). For both models the void fraction was 10^{-4} and Commander and Prosperetti model used Gaussian distributed bubbles with μ=200 μm and σ=100 μm.

Experiment Sites

The Laguna Madre is a long, shallow, hypersaline lagoon located between the mainland of South Texas and Padre Island. The experiment was conducted in the Lower Laguna Madre during 3 – 4 October 2018. In early October, T. testudinum is typically just past the annual peak of its above-ground biomass.
Data were collected at two sites located on the eastern side of the lagoon. The motivation in choosing these two sites was to have a seagrass site completely covered by a homogenous meadow of *T. testudinum*, and a seagrass-free site completely devoid of seagrass. Ideally the seagrass-free site would provide a control experiment designed to minimize the effects of variables (i.e., water depth, sediment type, water column variability, surface roughness) other than the independent variable (i.e., seagrass). However, such exemplary sites were not realized in the natural environment, and the experiment sites are approximations of these ideals.

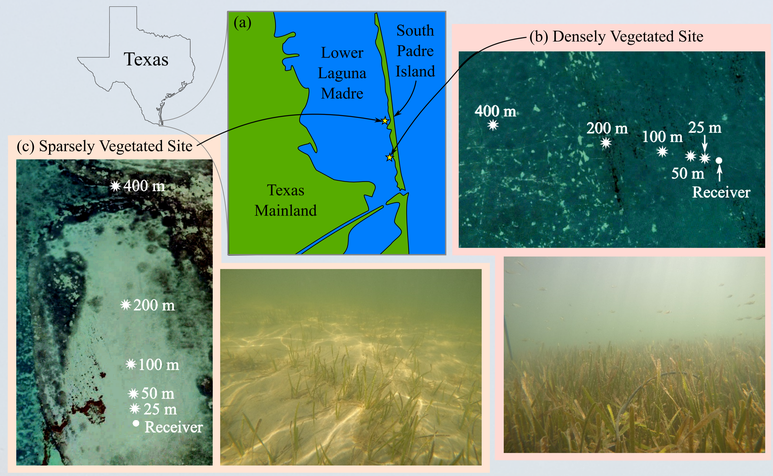

(a) Map of the Lower Laguna Madre with the locations of experiment sites indicated by stars. (b) Satellite imagery of the densely vegetated site with the location of the hydrophone receiver (circle) and source locations (stars), and a photograph of the seagrass coverage. (c) Satellite imagery of the sparsely vegetated site with the location of the hydrophone receiver (circle) and source locations (stars), and a photograph of the seagrass coverage.

Combustive Sound Source (CSS)

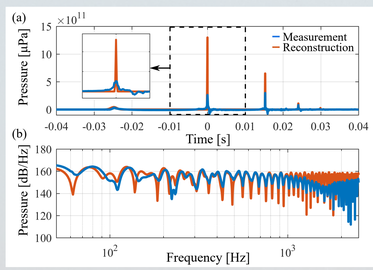

Top: (a) Measured and reconstructed source waveforms recorded at the sparsely vegetated site. Inset figure shows a closeup of the bubble collapse. (b) Spectra of the measured and reconstructed source waveforms.
Left: CSS chamber deployed in the seagrass meadow. The bottom of the chamber is open to the environment.

The Combustive Sound Source (CSS) produces a repeatable, broadband signal with peak frequency components below 100 Hz (Wilson et al., 1995). The CSS is comprised of three main components: a submersible combustion chamber, a gas delivery system, and an ignition system. The chamber was lowered to mid-depth in the water column and then filled with a stoichiometric ratio of hydrogen and oxygen gas. The gas was ignited by a spark plug positioned in the top of the chamber, causing the gas to turn into high temperature combustion products (mostly water vapor). The resulting bubble motion radiates acoustic pulses.
For both sites, acoustic data recordings of broadband signals from a CSS were recorded on a bottom-mounted hydrophone, deployed from an anchored monitoring boat. The CSS was deployed from a second boat along a transect at positions 25, 50, 100, 200, and 400 m away from the hydrophone. For the densely vegetated site, which was targeted as the primary interest for this work, the CSS signals were recorded at five separate times throughout the day. At the less vegetated site, one transect was conducted, with the measurements occurring mid-morning.

Supporting Environmental Measurements

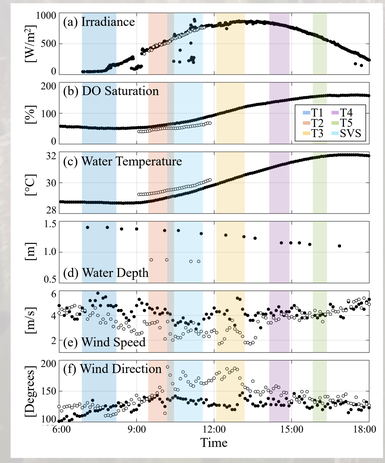

Measurements of solar irradiance were obtained using a pyranometer mounted on the stationary boat monitoring the hydrophone receivers. Solar irradiance began to increase just before 8:00 and reached a maximum level around 13:00. Measurements of dissolved oxygen and water temperature were obtained with a probe submerged near the lagoon floor. Both quantities are observed to increase during the course of the day, with a time lag relative to the solar irradiation of approximately three to four hours. Water depth was measured at the receiver positions using a marked rod, and tidal effects can be observed in the measurements. Wind direction and wind speed data from NOAA buoy 8779748 were obtained from the National Oceanic and Atmospheric Administration.

(a-d) Environmental parameters measured at the experiment sites and (e,f) by a NOAA weather buoy. In all plots, the data recorded at the densely vegetated site on October 3 are shown by the solid circles, and data recorded at the sparsely vegetated site on October 4 are shown by the open circles. The shaded areas represent the time periods during which the acoustic measurements were recorded. The horizontal axis is local time on October 3 for the measurements at the densely vegetated sites (listed as T1 – T5 in the legend) and local time on October 4 for the measurements at the sparsely vegetated site (listed as SVS in the legend).

Acoustic Measurements

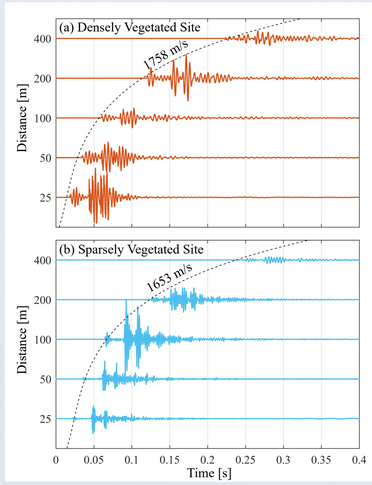

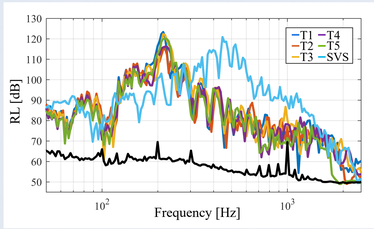

Left: Measured time series recorded at the (a) densely vegetated site (Transect 2) and (b) sparsely vegetated site. In both plots, the vertical axis is distance from source to receiver and is shown on a logarithmic scale. The received signals are multiplied by the source/receiver distance so their relative amplitudes can be compared. The dashed black line is a linear fit to the arrival of the signals, and the estimated wave speeds are listed near the curves.
Top: Frequency spectra for a single CSS reception from all five transects at the 100 m range at the densely vegetated site and at the sparsely vegetated site. There is very little variability between all the measurements recorded at the densely vegetated site. The differences in the shapes of the spectra between the densely and sparsely vegetated sites is driven by the mode cut-off frequency which is lower at the densely vegetated site due the lower effective sound speed in the bubbly liquid layer. The black curve is the average noise level.

Bayesian Inference

This work utilizes a Bayesian inference method to estimate the posterior probability distributions (PPDs) of environmental parameters **m**, from the measured acoustic data **d**. In a Bayesian formulation, the complete solution to an inference problem is characterized by the PPD of the unknown model parameters (Dosso and Nielsen, 2002).

Error function
(quantifies the difference between the measured and modeled data)

Conditional probability (represents the PPD) → $\mathcal{P}(\mathbf{m}|\mathbf{d}) \propto \frac{\exp[-\mathcal{E}](\mathbf{m})\mathcal{P}(\mathbf{m})}{\int \exp[-\mathcal{E}](\mathbf{m}')\mathcal{P}(\mathbf{m}')d\mathbf{m}'}$ ← Prior information (assume uniform distributions)

Error function is defined as the geometric mean between the normalized cross-correlation of the measured and modeled time series and the difference between the spectral levels in decidecadal bands of measured and modeled data.
The forward model uses a normal mode approach to calculate acoustic propagation in a layered medium using an effective sound speed and attenuation calculated using the Commander and Prosperetti model.

Estimated Marginal Probability Distributions

The narrowest distributions were found for the void fraction in the water layer. The MAP estimates of the void fraction for the five data sets recorded at the densely vegetated were more than five times greater than that of the sparsely vegetated site.
In addition to having a substantially lower MAP estimate, the marginal probability distribution for the void fraction at the sparsely vegetated site also shows much greater uncertainty than the values at the densely vegetated site. While the lower void fraction is attributed to the overall lower coverage of seagrass, the increased uncertainty is believed to be caused by range-dependence of seagrass coverage along the propagation path.
The marginal probability distributions for the bubble size parameters show a slight trend towards small bubbles with a narrow size distribution; however, overall, the marginals for the bubble size parameters are uninformative. The low-frequency data considered in the inversion are below the individual bubble resonance frequency. Within this frequency band, the effective sound speed is primarily inuenced by the void fraction, and it is less affected by the sizes of the bubbles.

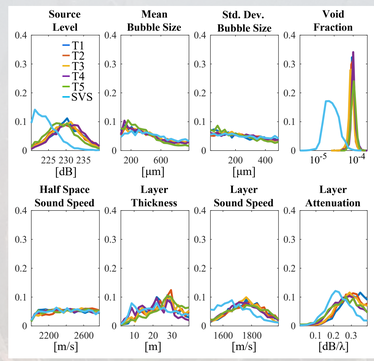

Marginal probability distributions of the inferred parameters determined for measurements at the densely vegetated sites (listed as Transects 1-5 in the legend) and at the sparsely vegetated site (listed as SVS in the legend).

Conclusions

These results demonstrate the potential use of acoustical methods to remotely sense seagrass productivity. The sensitivity of sound to the void fraction of gas present in the seagrass meadow was established by the narrow marginal probability distributions that provided distinct estimates of the void fraction between the densely and sparsely vegetated sites.
The Bayesian approach provided a comprehensive solution to the inference problem. The nonlinear approach allows for a complex representation of the environment, which included modeling the water layer as a bubbly liquid with a frequency-dependent sound speed and attenuation and a sediment layer over a semi-infinite acoustic half space. The PPD of the unknown model parameters and the marginal probability distributions were examined to indicate the resolution of the estimated void fractions.
A comparison of the void fractions estimated at the densely vegetated and sparsely vegetated sites showed that the estimate void fractions were well-resolved. Within the densely vegetated site, the distributions were overlapping, and although the map estimates indicated a slight increase in the estimated void fraction during the periods of highest irradiance, the diurnal changes are within the uncertainty of the estimates.

Diurnal Effects

Short-range data were simultaneously collected at both the densely and sparsely vegetated sites (Lee et al., 2019). The measurements were collected over a wider frequency band (0.1 kHz to 100 kHz), which allowed for identification of an excess attenuation band that occurred from 3.5 kHz to 35 kHz in the afternoon when bubble production from photosynthesis was at a maximum. A comparison of the measurements between the two sites revealed the received signal level was 25 dB higher at the sparsely vegetated site, in terms of spectral level averaged over the entire frequency band. For frequencies below 2.5 kHz, no discernible diurnal changes in the received signal level were observed. These observations led to the hypothesis that bubbles within the seagrass tissue were primarily responsible for the difference in low-frequency acoustic propagation effects between the sparsely and densely vegetated sites.

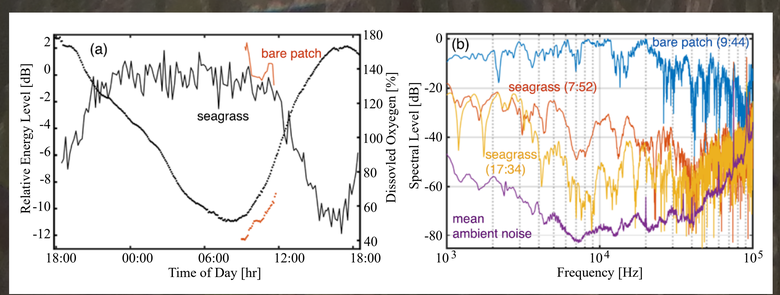

(a) Changes in received acoustic energy (solid lines, left horizontal axis) and dissolved oxygen (circles, right horizontal axis) vs time of day. Data are shown for the seagrass bed and the bare patch. To place the bare patch data on the same scale as the seagrass data, a horizontal offset of 24 h was applied to all of the bare patch data, and a vertical offset of -30 dB applied to the bare patch acoustic data. (b) Spectral levels for the bare patch (time of day = 9:44, dissolved oxygen = 41%), seagrass bed early in the morning (time of day = 7:52, dissolved oxygen = 51%) and late afternoon (time of day = 17:34, dissolved oxygen = 152%), and mean ambient noise level in the seagrass bed for the 24 h experiment period.

Acknowledgements

This work was supported by the ARL:UT Independent Research and Development Program and by the Office of Naval Research (ONR) Ocean Acoustics Program under Grants No. N00014-18-1-2401 and N00014-18-1-2227.

References

Commander KW, Prosperetti A (1989) Linear pressure waves in bubbly liquids: Comparison between theory and experiments. J Acoust Soc Am 85(2):732-746.
Dosso SE, Nielsen PL (2002) Quantifying uncertainty in geoacoustic inversion. I. A fast Gibbs sampler approach. J Acoust Soc Am 111(1):143-159.
Lee KM, Ballard MS, Venegas GR, Sagers JD, McNeese AR, Johnson JR, Wilson PS, Rahman AF (2019) Broadband sound propagation in a seagrass meadow throughout a diurnal cycle. J Acoust Soc Am 146:EL335-EL341.
Mallock A (1910) Damping of sound by frothy liquids. Proc Roy Soc 84:391-395.
Wood AB (1930) A Textbook of Sound, 2nd edn. Bell, London.
Wilson PS, Ellzey JL, Muir TG (1995) Experimental investigation of the combustive sound source. IEEE J Oceanic Eng 20(4):311-320.